GENERATION AND TOOTH CONTACT ANALYSIS (TCA) OF HYPOID GEAR DRIVE

Assist. Prof. Mohammad Q. Abdullah
Dep. Of Mech.
College of Engineering
University of Baghdad

Nassear R. Hmoad

ABSTRACT

The present work covers the Face-Hobbing method for generation and simulation of meshing of Face hobbed hypoid gear drive. In this work the generation process of hobbed hypoid gear has been achieved by determination of the generation function of blade cutter. The teeth surfaces have been drawn depending on the simulation of the cutting process and the head cutter motion. Tooth contact analysis (TCA) of such gear drive is presented to evaluate analytically the transmission error function for concave and convex tooth side due to misalignment errors. TCA results show that the gear is very sensitive to misalignment errors and the increasing of the gear teeth number decrease the transmission error for both concave and convex tooth sides and ensure smooth motion with low vibration.

الخلاصة

العمل الحالي يغطي طريقة توليد ومحاكاة التعشيق للتروس المخروطية ذات الاسنان الحلزونية الأسفينية. في هذا العمل تمت عملية توليد المسنن بأيجاد معادلة توليد شفرة القطع. رسمت اسطح السن اعتمادا على محاكاة عملية القطع وحركة شفرة القطع. تم تقديم الوصف التحليلي لتماس الاسنان لأيجاد دالة خطأ النقل لجانب السن المقعر والمحدب لهذا النوع من المسننات نتيجة عدم تطابق تعشيق التروس. نتائج تحليل تلامس السن تبين ان المسنن حساس جدا لأخطاء التطابق وأن زيادة عدد الاسنان تقلل اخطاء نقل الحركة وتضمن حركة سلسة مع تقليل الأهتزاز .

KEYWORD

Hypoid, Generation, Tooth Contact Analysis (TCA).

Introduction:

Generation of hypoid bevel gears depends upon the theory of derivation of gear and pinion tooth surface. The accurate geometrical representation of gear tooth surface is the first step to design a successful gear drive. This paper presents a mathematical model able to compute the tooth surface of hypoid gear drive cut by face-hobbing method (FH). At first a brief discussion about kinematic relationships of FH process and about the main characteristics of face-hobbed tooth cutting tools will be proposed. Then the cutting tools will be described analytically, after that according to the theory of gearing the cutting process will be simulated and gear tooth surface will be derived.

1- Face Hobbing Method:

In Fig. (1) FH process are shown schematically. The head cutter is provided with (N_c) groups of blade. Each group contains three blades, one for rough cutting and two finishing blades one for each tooth side [**F. L. Litvin , 1991**]. To accomplish continuous indexing, the head cutter and the being cut gear are rotated in opposite directions. While the head cutter is rotated by the angle ($2\pi/N_c$) the gear is rotated through the angle ($2\pi/N_i$), where (N_i) is gear or pinion teeth number. Thus the next group of blades will start to cut the next gear tooth after finishing the current tooth, according to that the rotation of the cutter (θ_c) is related to that of work piece(θ_i) by the ratio (R_b).

$$R_b = N_c/N_i = \theta_i/\theta_c \qquad (1)$$

2- Analytical Description of Cutting Blade Geometry:

The analytical description will be focused on the two finishing blades only, which shaped the gear tooth surfaces. Fig. (2) shows, from two different viewpoints, the location of one blade group in Gleason Tri-ac left-handed (LH) head cutter. A left-handed gear or pinion is cut by a (LH) head cutter [**V. Simon and U. L. Hungary, 2000**]. Fig. (3) shows the outer and inner cutting blades of straight edge without filet. There are three reference coordinate systems to specify the blade geometry as below.

1. S_e- Fixed at the pitch point (P) and its axes parallel to the edge of the tool blank.
2. S_b- Its origin at (P), (x_b) coinciding with (x_e) , (y_b) and (z_b) having hook angle (η_b) with(y_e) and (z_e).
3. z_t- Its origin has been setup at the tip of the blade and its

components parallel to (s_b)components.

(α_e) presents blade angle (pressure angle) between the projection of the cutting edge on ($x_e z_e$) plane and(z_e). The cutting edge lies entirely on a plane, called rake plane, which forms rake angle (k_e), usually equal to 12°, with tool blank plane having as normal the (y_e) axis. Hook angle (η_b), usually equal to 4.42°, represent the direction of cutting blade with respect to the head cutter rotation axis (z_h). The eccentric angle (ε_b) is the angle between (s_b) and (s_h) coordinate systems.

At first a vector (c_e) oriented along the cutting edge and pointing from point (P) to the blade tip will be defined in (s_h) system. The upper sign refers to the outer blade and the lower one refers to inner blade, [**V. Simon and U. L. Hungary, 2000**]

$$c_e = \begin{bmatrix} \pm sin\,(\alpha_e) \\ sin(\alpha_e)\,tan\,(k_e) \\ cos\,(\alpha_e) \end{bmatrix} \quad (2)$$

The normal unit vector to rake plane is.

$$n_e = \begin{bmatrix} \pm sin\,(k_e \\ -cos\,(k_e) \\ 0 \end{bmatrix} \quad (3)$$

The representations of c_e, n_e, α_e , and k_e in (s_b) system are [**V. Simon and U. L. Hungary, 2000**].

$$c_b = \begin{bmatrix} c_{bx} \\ c_{by} \\ c_{bz} \end{bmatrix} = \begin{bmatrix} 1 & 0 & 0 \\ 0 & cos\,(\eta_b) & -sin\,(\eta_b) \\ 0 & sin\,(\eta_b) & cos\,(\eta_b) \end{bmatrix} c_e \quad (4)$$

$$n_b = \begin{bmatrix} n_{bx} \\ n_{by} \\ n_{bz} \end{bmatrix} = \begin{bmatrix} 1 & 0 & 0 \\ 0 & cos\,(\eta_b) & -sin\,(\eta_b) \\ 0 & sin\,(\eta_b) & cos\,(\eta_b) \end{bmatrix} n_e \quad (5)$$

$$\alpha_b = tan^{-1}\,(\pm c_{bx}/c_{bz}) = f(\alpha_e, k_e, \eta_b) \quad (6)$$

$$k_b = tan^{-1}(\pm c_{by}/c_{bx}) = f\,(\alpha_e, k_e, \eta_b) \quad (7)$$

Eccentric angle found to be calculated as in Eq. (8), [**F. L. Litvin , 1989**]

$$\varepsilon_b = sin^{-1}(N_c\, r_i\, cos\,(\beta_i)/(N_i) * r_b) \quad (8)$$

Where (r_i) presents gear radius if (i =1) and pinion radius if (i =2), and (β) is spiral angle, r_b is the cutter radius. The measured c_b, n_b and α_b in s_h systems are.

$$c_h = \begin{bmatrix} c_{hx} \\ c_{hy} \\ c_{hz} \end{bmatrix} = \begin{bmatrix} \cos(\varepsilon_b) & \sin(\varepsilon_b) & 0 \\ -\sin(\varepsilon_b) & \cos(\varepsilon_b) & 0 \\ 0 & 0 & 1 \end{bmatrix} c_b \quad (9)$$

$$n_h = \begin{bmatrix} n_{hx} \\ n_{hy} \\ n_{hz} \end{bmatrix} = \begin{bmatrix} \cos(\varepsilon_b) & \sin(\varepsilon_b) & 0 \\ -\sin(\varepsilon_b) & \cos(\varepsilon_b) & 0 \\ 0 & 0 & 1 \end{bmatrix} n_b \quad (10)$$

$$\alpha_h = \tan^{-1}(\pm c_{hx}/c_{hz}) = f(\alpha_g, k_g, \eta_b, \varepsilon_b) \quad (11)$$

The above eq.s are the analytical description of cutting blade geometry. Fig. (4) shows more complex blade shape consists of four sections and these sections are.

(I)- Bottom: straight horizontal segment.

(II)- Fillet: circular arc of radius (r_g, fillet radius) and center at (R).

(III)- Toprem: straight inclined segment with length (L_T) and angle (τ).

(IV)- Curved blade: a circular arc with radius (ρ) and center at point (O).

The coordinates of (P) are [**V. Simon and U. L. Hungary, 2000**].

Where the upper sign refers to right side of the plade and the lower sign refers to the left side of the plade

$$\left.\begin{aligned} x_p &= \pm h_f \tan(\alpha_b) \\ y_p &= -h_f \tan(\alpha_b) \tan(k_b) \end{aligned}\right\} \quad (12)$$

$$z_p = -h_f$$

Point (A) the intersection of (x_t) with the toprem section there for the distance of (OA) is

$$OA = \sqrt[2]{\rho_t^2 + L_T^2 - 2\,\rho_t\, L_T \cos\left(\frac{\pi}{2} - \tau\right)} \quad (13)$$

Where (ρ_t) is the projection of (ρ) on (x_t, z_t) plane and (τ) is toprem angle.

$$A\bar{O}B = \sin^{-1}(L_T \sin(\pi/2 - \tau)/OA) \quad (14)$$

The intersection of the circular arc with the Toprem occurs at point (B). The angle between (OA) and (x_t) is, [**V. Simon and U. L. Hungary, 2000**]

$$\lambda = \sin^{-1}(z_o/OA) \quad (15)$$

Then the coordinates of (A) are

$$\left.\begin{aligned} x_A &= x_O \pm OA\cos(\lambda) \\ z_A &= 0 \\ y_A &= 0 \end{aligned}\right\} \quad (16)$$

$$\delta = \lambda + A\hat{O}B \quad (17)$$

$$\gamma = \pi/2 - (\delta - \tau) \quad (18)$$

$$L_1 = r_e\,\gamma \quad (19)$$

$$\left.\begin{aligned} x_R &= x_A \pm r_e \tan(\gamma/2) \\ z_R &= -r_e \end{aligned}\right\} \quad (20)$$

Toprem length can be calculated as

$$L_2 = L_T - r_e \tan(\gamma/2) \quad (21)$$

The calculation of cutting edge in (s_t) system depends on the blade section to be calculated, Table (1) propose the calculation of blade sections in (s_t).

All points of cutting edge lie in the rake plane and (y_t^p) can be obtained as

$$y_t^p(s) = y_p z + \left[\left(x_p - x_t^p(s)\right)n_{bx} + \left(z_p - z_t^p(s)\right)n_{bz}\right]/n_{by} \quad (22)$$

And the cutting blade representation in head cutter center is

$$r_h^p(s) = \begin{bmatrix} r_b + \left(x_t^p(s) - x_p\right)\cos(\varepsilon_b) + \left(y_t^p(s) - y_p\right)\sin(\varepsilon_b) \\ -\left(x_y^p(s) - x_p\right)\sin(\varepsilon_b) + \left(y_t^p(s) - y_p\right)\cos(\varepsilon_b) \\ z_t^p(s) - x_p \end{bmatrix} \quad (23)$$

3- Simulation of FH Cutting Process:

Eq. (23) represents the principle point to start the simulation process. According to gearing theory the proper coordinate transformation able to simulate the cutting process and compute the gear drive teeth surfaces. Simulation process has two forms depending upon generating or non-generating cutting process.

3.1- FH Cutting Process Without Generation:

Fig. (5) show FH cutting machine which is setup to cut format gear member. A proper set of reference frames has to be introduced in order to describe the machine setting. There are three machine reference coordinate systems (s_h) which has been specified previously, (s_m) its origin at (o_m) and (z_m) parallel to (z_h), (s_w) which has been setup with its origin at $(o_w$, gear apex) where (z_w) coincides with the gear rotation axis. When the cutter rotates by angle (θ) gear rotation will be $(R_b\ \theta)$ condition of continuous indexing.

Gleason saved files (SAF) provides the details to properly locate, with respect to reference frame (s_m) machine root angle (γ_m) and machine center to back (Δx_p). The setting (H) and (V) found to be a function of gear drive shape parameters as in eq.s (24) and (25), [**F. L. Litvin etal, 1991**].

$$V = r_b \cos(\beta - \varepsilon_b) \quad (24)$$

$$H = (r_i / \sin(\gamma_m)) - r_b \sin(\beta - \varepsilon_b) \quad (25)$$

Finally the representation of gear tooth surfaces is

$$r_2^p(\theta, s) = M_{w2}\, M_{2m}\, M_{m1}\, M_{1h}\, r_h^p(s) \quad (26)$$

where

$$M_{m1} = \begin{bmatrix} \cos\theta & \sin\theta & 0 \\ -\sin\theta & \cos\theta & 0 \\ 0 & 0 & 1 \end{bmatrix},$$

$$M_{m1} = \begin{bmatrix} 1 & 0 & 0 \\ 0 & 1 & 0 \\ 0 & 0 & 1 \end{bmatrix} + \begin{bmatrix} H \\ \pm V \\ 0 \end{bmatrix}$$

$$M_{2m} = \begin{bmatrix} \cos(\frac{\pi}{2} - \gamma_m) & 0 & \sin(\frac{\pi}{2} - \gamma_m) \\ 0 & 1 & 0 \\ -\sin(\frac{\pi}{2} - \gamma_m) & 0 & \cos(\frac{\pi}{2} - \gamma_m) \end{bmatrix} + \begin{bmatrix} 0 \\ 0 \\ -\Delta X_p \end{bmatrix}$$

,

$$M_{w2} = \begin{bmatrix} \cos(R_b\theta) & \sin(R_b\theta) & 0 \\ -\sin(R_b\theta) & \cos(R_b\theta) & 0 \\ 0 & 0 & 1 \end{bmatrix}$$

In Fig. (6) a non-generated gear blank is drown depending upon eq. (26) by using the Gleason SAF details (γ_m, Δx_p).

The normal vector to these surfaces which is used to analyze tooth contact analysis is

$$n_2^p(\theta, s) = \frac{\partial}{\partial s} r_w^p(\theta, s) \times \frac{\partial}{\partial \theta} r_w^p(\theta, s) \quad (27)$$

3.2- FH Cutting Process with Generation Motion:

Theoretically FH with generation motion is based on a generalized concept of bevel gear generation in which the pinion is generated by a complementary generation crown gear. The tooth surfaces of the generating crown gear are kinematicly formed by the traces of the head cutter edge and the cradle rotation, [**Dr.Qi Fan, 2007**], cradle is a mechanical element centered at (o_m) and carrying the head cutter. In generated FH method there are two sets of related motion are defined. The first set was specified in eq. (1), the second set presents the rotation of the cradle and the pinion as below

$$R_a = N_g / N_1 = \theta_1 / \phi \quad (28)$$

(R_a) represents the roll ratio, (N_g) is the generating crown gear teeth number, (ϕ) is the crown gear rotation. Fig. (7) show FH cutting machine which is ready to cut the generated pinion. It is seen that the reference coordinate systems (s_h), (s_m) and (s_m) have been rigidly connected respectively to the head cutter, machine center and work piece. The (s_c) system rigidly connect to the cradle. The rotation of

pinion is a function of (θ) and cradle rotation (ϕ).

$$\theta_1 = R_b\,\theta + R_a\,\phi \qquad (29)$$

Radial setting (s_r) and cradle angle (q) can be computed as in eq.s (30) and (31).

$$s_r = \sqrt[2]{H^2 + V^2} \qquad (30)$$

$$q = tan^{-1}(V/H) \qquad (31)$$

The Gleason SAF kept the values of (R_a) and of all the setting to properly locate, with respect to the reference frame (s_m), the pinion setting

E_m: pinion offset ,γ_m: machine root angle ,Δx_b: sliding base , i : tilt angle ,j : swivel angle

The cutting edges representation in (s_w) is derived in eq. (32)

$$r_1^p(\theta,\phi,s) = M_{ws}\,M_{54}\,M_{4m}\,M_{mc}\,M_{c3}\,M_{32}\,M_{21}\,M_{1h}\,r_h^p(s) \qquad (32)$$

Where

$$M_{1h} = \begin{bmatrix} \cos\theta & \sin\theta & 0 \\ -\sin\theta & \cos\theta & 0 \\ 0 & 0 & 1 \end{bmatrix},$$

$$M_{21} = \begin{bmatrix} \cos i & 0 & \sin i \\ 0 & 1 & 0 \\ -\sin i & 0 & \cos i \end{bmatrix},$$

$$M_{32} = \begin{bmatrix} \cos j & \mp\sin j & 0 \\ \pm\sin j & \cos j & 0 \\ 0 & 0 & 1 \end{bmatrix}$$

$$M_{c3} = \begin{bmatrix} \cos\left(\frac{\pi}{2}-q\right) & \mp\sin\left(\frac{\pi}{2}-q\right) & 0 \\ \pm\sin\left(\frac{\pi}{2}-q\right) & \cos\left(\frac{\pi}{2}-Aq\right) & 0 \\ 0 & 0 & 1 \end{bmatrix} + \begin{bmatrix} 0 \\ \mp s_r \\ 0 \end{bmatrix},$$

$$M_{mc} = \begin{bmatrix} \cos\phi & \sin\phi & 0 \\ \sin\phi & \cos\phi & 0 \\ 0 & 0 & 1 \end{bmatrix}$$

$$M_{4m} = \begin{bmatrix} 1 & 0 & 0 \\ 0 & 1 & 0 \\ 0 & 0 & 0 \end{bmatrix} + \begin{bmatrix} 0 \\ \pm E_m \\ -\Delta X_b \end{bmatrix},$$

$$M_{54} = \begin{bmatrix} \cos(\frac{\pi}{2}-q) & 0 & \sin(\frac{\pi}{2}-q) \\ 0 & 1 & 0 \\ -\sin(\frac{\pi}{2}-q) & 0 & \cos(\frac{\pi}{2}-q) \end{bmatrix} + \begin{bmatrix} 0 \\ 0 \\ -\Delta X_p \end{bmatrix}$$

$$M_{ws} = \begin{bmatrix} \cos(R_b\theta + R_b\phi) & \sin\cos(R_b\theta + R_b\phi) & 0 \\ -\sin\cos(R_b\theta + R_b\phi) & \cos\cos(R_b\theta + R_b\phi) & 0 \\ 0 & 0 & 1 \end{bmatrix}$$

Eq. (32), unlike eq. (26), is not surface but represents family of surfaces. In order to drive the tooth surfaces it is necessary to calculate the set of points for whom, the eq. (33), which represents the tooth surface points, satisfied [**F. L. Litvin etal, 1991**].

$$\frac{\partial}{\partial s} r_1^p(\theta,\phi,s) \times \frac{\partial}{\partial \theta} r_1^p(\theta,\phi,s)) \cdot \left(\frac{\partial}{\partial \phi} r_1^p(\theta,\phi,s)\right) = 0 \qquad (33)$$

By using a proper values that satisfy eq. (32) and (33) each part of the tooth surface is generated. The normal vector to these surfaces is obtain by eq. (34)

$$n_1^p(\theta,\phi,s) = \frac{\partial}{\partial s} r_1^p(\theta,\phi,s) \times \frac{\partial}{\partial \theta} r_1^p(\theta,\phi,s) \quad (34)$$

Fig. (8) shows hypoid pinion blank, the two meshed gears are shown in Fig. (9).

4 - Determination of Transmission Error:

The transmission function of an ideal gear drive is a linear one which is depends on ratio of gear teeth number

$$\theta_2 = \frac{N_1}{N_2}\theta_1 \quad (35)$$

Due to misalignment between the meshing gears the real transmission function $\theta_2(\theta_1)$ becomes piecewise periodic function with the period equal to the cycle of meshing of a pair of teeth. Due to The jump of angular velocity at the junction of cycles the acceleration approaches to large value of acceleration that cause large vibration and noise, for this reason it is necessary to predesign a parabolic function of transmission error that can absorb a linear function of transmission error and reduce the jump of angular velocity and acceleration [**F. L. Litvin and Yi Zhang, 1991**] and [**F. L. Litvin, 2006**]. The linear transmission function and the predesigned function are in tangency at the mean contact point and have the same derivative (m_{21}) at this point.

$$m_{12} = \partial\theta_2/\partial\theta_1 = N_1/N_2 \quad (36)$$

The predesigned transmission function is represented as

$$\theta_2 - \theta_2^{(0)} = F(\theta_1 - \theta_1^{(0)}) \quad (37)$$

Here ($\theta_1^{(0)}$) and ($\theta_2^{(0)}$) are the initial angles of rotation of pinion and gear that provide the tangency of gear tooth surfaces a mean contact point (M). By using the Taylor expansion up to the members of second order, [**F. L. Litvin, 2006**].

$$F(\theta_1 - \theta_1^{(0)}) = \frac{\partial}{\partial\theta_2} F(\theta_1 - \theta_1^{(0)}) + .5 \frac{\partial^2}{\partial\theta^2} F(\theta_1 - \theta_1^{(0)})$$

$$= m_{21}(\theta_1 - \theta_1^{(0)}) + .5\,\acute{m}_{21} \quad (38)$$

($\acute{m}_{21}$) is the to be chosen constant value: positive for the gear concave side, and negative for the gear convex side. The synthesized gears rotates with a parabolic function of transmission errors represented by

$$\Delta\theta_2(\theta_1) = .5\,\acute{m}_{21}(\theta_1 - \theta_1^{(0)})^2 \quad (39)$$

Where

$$-\pi/N_1 \le (\theta_1 - \theta_1^{(0)}) \le \pi/N_2$$

Eq. (39) enables the determination of ($\acute{m}_{21}$), considering as known the expected values of transmission errors [**F. L. Litvin, 1989**]. Eq. (39) has another form of second order

function [**Dr. Q. Fan and Dr. L. Wilcox, 2006**].

$$\Delta\theta_2(\theta_1) = a_t + b_t(\theta_1 - \theta_1^{(0)}) - c_t(\theta_1 - \theta_1^{(0)})^2 \quad (40)$$

5- Results and Discussions of Tooth Contact Analysis (TCA):

All the results of tooth contact that has been shown in Fig.s (11)--(19) specify the shape and magnitude of transmission errors for both tooth concave and convex side for different teeth number. These results are based on eq. (40) and by using the maximum transmission errors presented in [**T. J. Maiuri , 2006**], [**V. Simon and U. L. Hungary, 2000**]. The pinion has been shifted along its axis by $\pm\Delta P$ and also the misalignment can be achieved by changing the center distance ($\pm\Delta E$) which means the error of pinion shaft offset as shown in Fig. (9). The results show that the hypoid bevel gear is so sensitive to assembly errors, both misalignment procedures show that the transmission error functions have a linear or almost linear shape far away the mean contact point, the increasing of teeth number minimize the transmission error significantly and vibration will appear in every cycle of meshing. The misalignment for convex side is ΔE=0.508 mm, ΔP=-0.254 mm, and for concave side is ΔE=.254 mm, ΔP=-0.102 mm.

The gear and pinion machine- tool settings are shown in Table (3) and (4) respectively.

6- Conclusions:

The main conclusions obtained from the present work can be summarized as follow:

1. The modified mathematical model for tooth surface representation of face hobbed hypoid gear and its application for computerized design of these gears have been presented.

2. From tooth contact result its clear that:

   i. The hypoid gear drive is very sensitive to misalignment of their meshing.
   ii. The parabolic shape of transmission function have a linear shape far away the mean contact point.
   iii. The increasing of gear teeth number minimizes the transmission errors and ensure smooth transmission performance and low noise.

REFERENCES

F. L. Litvin, (Theory of gearing), NASA publication, 1212, AVSCOM technical report, 88-c-035, 1989.

F. L. Litvin, W.S. Chaing, C. Kuan, M. Lundy and W. J. Tsung, (generation and geometry of hypoid gear member with face-hobbed tooth of uniform depth), IVSL / ElSEVIER, Int. J. Mach. Tools Manufact. Vol. 31, No. 2, pp. 167-181, 1991.

F. L. Litvin and Yi Zhang, (Local synthesis and tooth contact analysis of Face-Milled spiral bevel gears), NASA, Technical report 4342,1991.

V. Simon, u. l. Hungary, (FEM stress analysis in hypoid gears), IVSL / PERGAMON, Mechanism and Machine theory, pp. 1197-1220, 2000.

Dr. Q. Fan and Dr. L. Wilcox, (New developments in tooth contact analysis (TCA) and loaded TCA for spiral bevel and hypoid gear drives), Journal, Available on line at WWW.geartechnology.com , 2006.

T. J. Maiuri. (Spiral bevel and hypoid Gear cutting technology update), WWW.geartechnology 2006.

F. L. Litvin, (Development of gear technology and theory of gearing), University of Illinois at Chicago, Chicago, Illinois.NASA RP-1406, taken at 2006.

Dr.Q. Fan, (Kinematical simulation of face hobbing and tooth surface generation of spiral bevel and hypoid gears), Journal, Avilable on line at WWW.geartechnology.com, 2007.

NOMENCLATURES

Symbol	Description	Unit
c_b	Cutting edge description in s_b system	---
c_e	Cutting edge description in s_e system	---
c_h	Cutting edge description in s_h system	---
E_m	Pinion offset	mm
h_f	Blade height	mm
H	Machine horizontal setting	mm
i	Tilt angle	degree
j	Swivel angle	degree
n_b	Cutting edge unit normal in s_b	---
n_e	Cutting edge unit normal in s_e	---
n_h	Cutting edge unit normal in s_h	---
$n_1^p(\theta,\phi,s)$	Normal of pinion tooth surfaces	---
$n_2^p(\theta,s)$	Normal vector of gear tooth surfaces	---
N_1	Pinion tooth number	---
N_2	Gear tooth number	---
N_c	Cutting blade number	---
N_g	Crown gear teeth number	---
r_b	Cutter radius	mm
r_e	Filet radius	mm
$r_h^p(s)$	Description of deferent cutting sections	mm
$r_1^p(\theta,\phi,s)$	Pinion toot surfaces	mm

$r_2^p(\theta, s)$	Gear tooth surfaces	mm
R_b	Ratio of gear drive rotation	---
V	Machine vertical setting	mm
α_b	Pressure angle in s_b	degree
α_e	Pressure angle	degree
α_h	Pressure angle in s_h	degree
β_1	Pinion spiral angle	degree
β_2	Gear spiral angle	degree
γ	Cutting blade filet angle	degree
γ_m	Pitch angle	degree
ε_b	Eccentric angle	degree
η_b	Hook angle	degree
$\theta_2^{(0)}, \theta_1^{(0)}$	Initial angle of rotation for gear and and pinion	degree
$\Delta\theta_2(\theta_1)$	Error transmission function	degree
τ	Toprem angle	degree

Table (1), calculation of different blade sections in (s_t) coordinate system.

Blade part	p	s^p	$\begin{Bmatrix} x_t^p(s) \\ z_t^p(s) \end{Bmatrix}$
Bottom	I	$s^1 \leq 0$	$\begin{Bmatrix} \pm s^I + x_R \\ 0 \end{Bmatrix}$
Fillet	II	$0 \leq s^{II} \leq L_1$	$\begin{Bmatrix} x_R \pm r_e \sin(s^{II}/r_e) \\ -r_e(1-\cos(s^{II}/r_e)) \end{Bmatrix}$
Toprem	III	$L_1 \leq s^{III} \leq L_1 + L_2$	$\begin{Bmatrix} x_R \pm r_e \sin(s^{III}/r_e) \pm (s^{III} - L_1)\sin(\delta - \tau) \\ -r_e(1-\cos(s^{III}/r_e)) - (s^{III} - L_1)\cos(\delta - \tau) \end{Bmatrix}$
Curved blade	IV	$L_1 + L_2 \leq s^{IV}$	$\begin{Bmatrix} x_O \pm \rho_t \cos(\delta + (s^{IV} - L_1 - L_2)/\rho_t) \\ z_O - \rho_t \sin(\delta + (s^{IV} - L_1 - L_2)/\rho_t) \end{Bmatrix}$

Table (2), Hypoid gear design data.

	Pinion	Gear
Number of teeth	12	30
Module (mm)	6	6
Running offset (mm)	15	
Outside diameter (mm)	72	180
Face width (mm)	31	27
Mean spiral angle (deg.)	30	20
Pitch angle (deg.)	18.5	71.5

Table (3), Gear machine- tool settings.

Cutter radius (mm).	75.184
Cutter blade angle (deg.)	17
Point width (mm)	2.032
Basic machine root angle γ_m (deg.)	64.5986
Machine center to back (ΔX_p) (mm)	2.358

Table (4), Pinion machine- tool setting,(for concave and convex side)

Setting	Value
Cutter radius (mm)	75.5
Cutter blade angle (deg.)	17
Machine root angle (deg.)	-3.44
Basic tilt angle (deg.)	21.22
Basic swivel angle (deg.)	-34.18
Basic cradle angle (deg.)	79.81
Sliding base setting (deg.)	16.498
Machine center to back (mm)	-1.117
Blank offset setting (mm)	23.411
Ratio of roll	3.5510

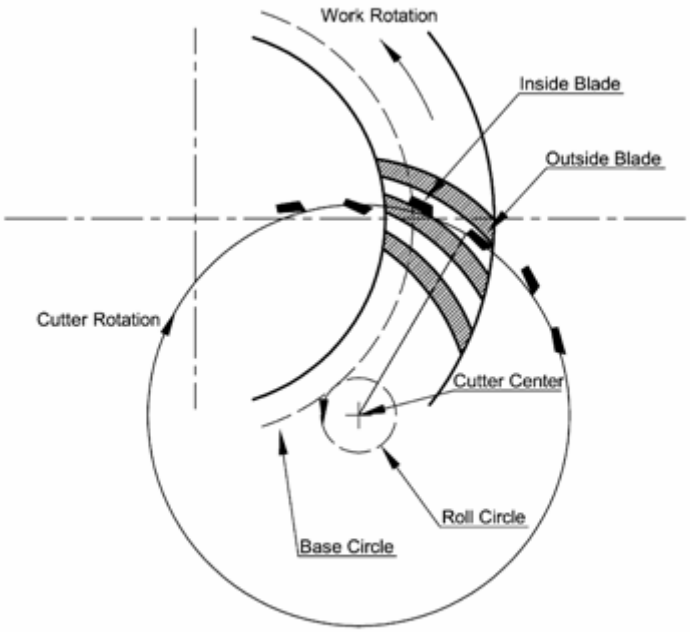

Fig. (1). Face Hobbing process

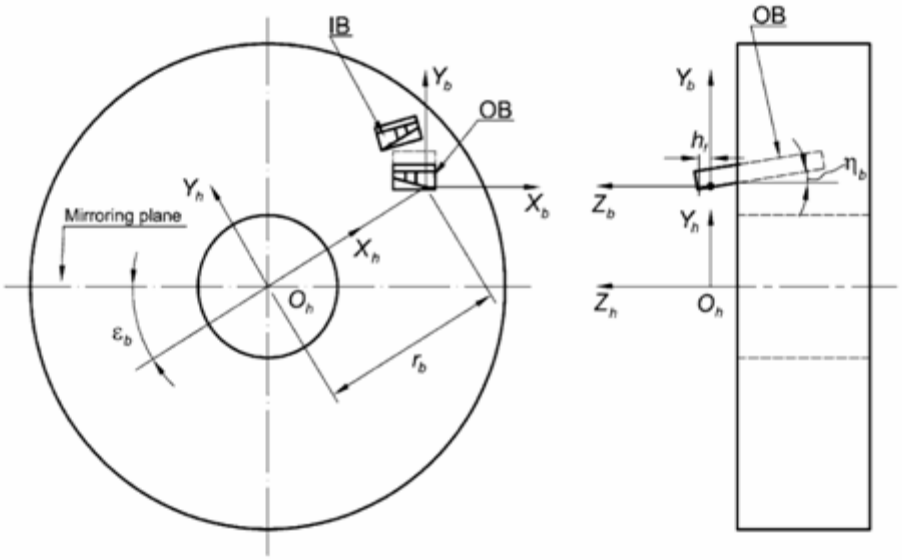

Fig. (2), LH blade group mounted in the head cutter .

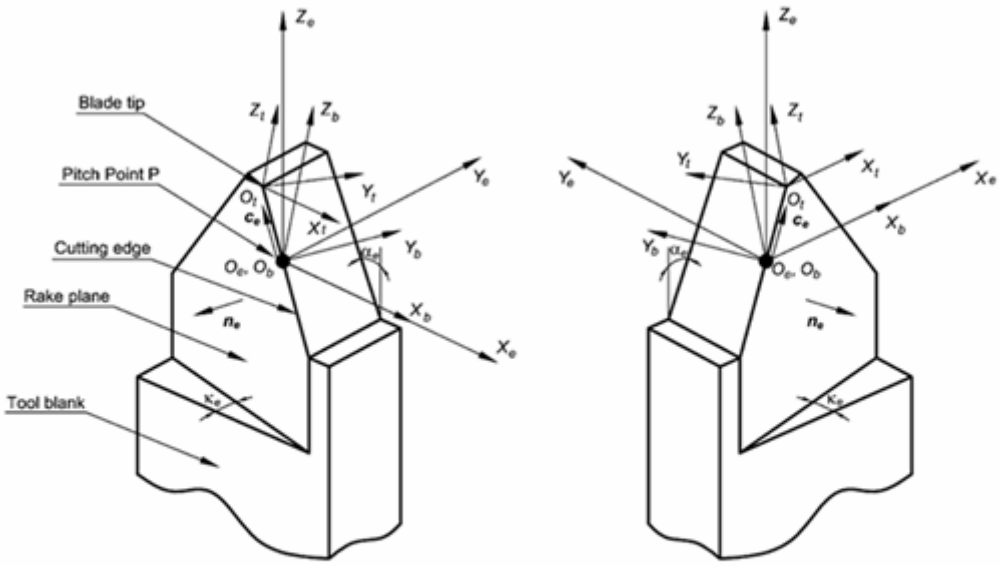

LH outer blade LH inner blade

Fig. (3), LH group blades .

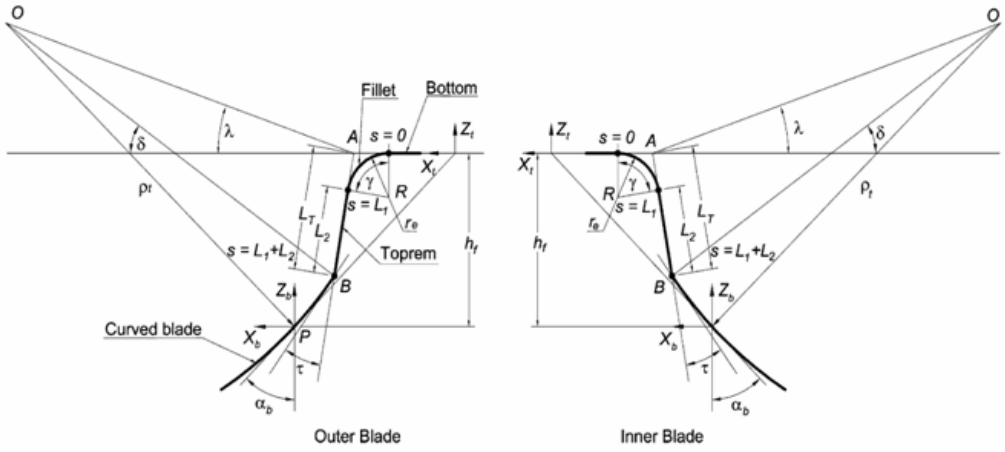

Outer blade Inner blade

Fig. (4) projection of the curved LH on x_t, z_t plane .

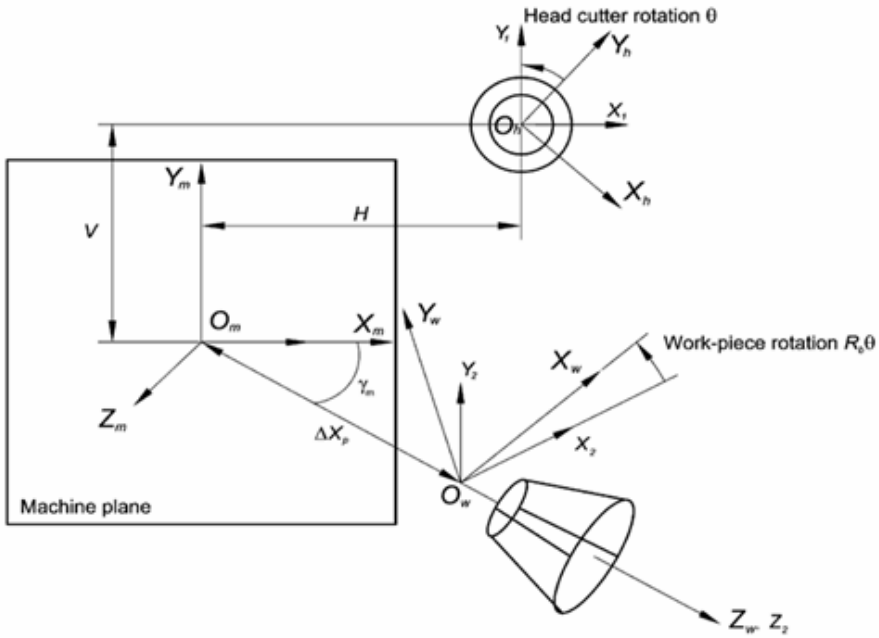

Fig. (5) cutting machine setup for cutting non-generated gear.

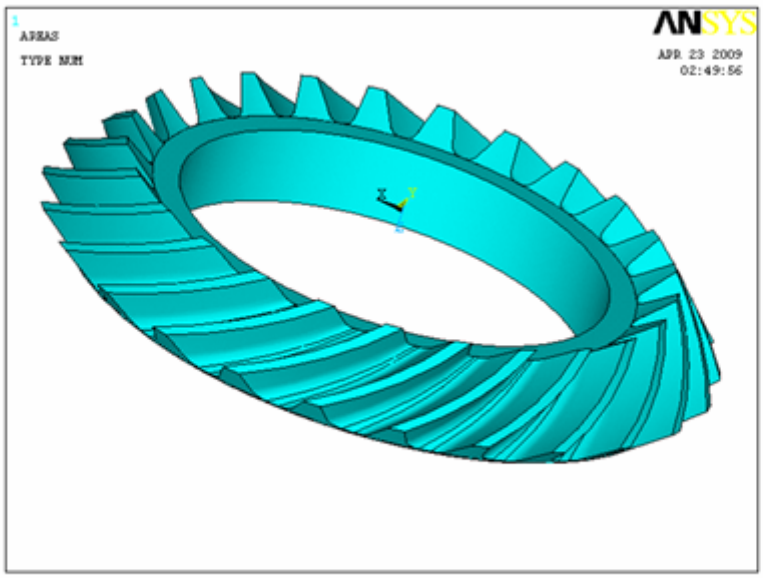

α = 22 degree

β = 30 degree

γ = 60 degree

r =90 mm

h_f = 4 mm

N_2 = 25

Fig. (6) (a), A non-generated gear blank

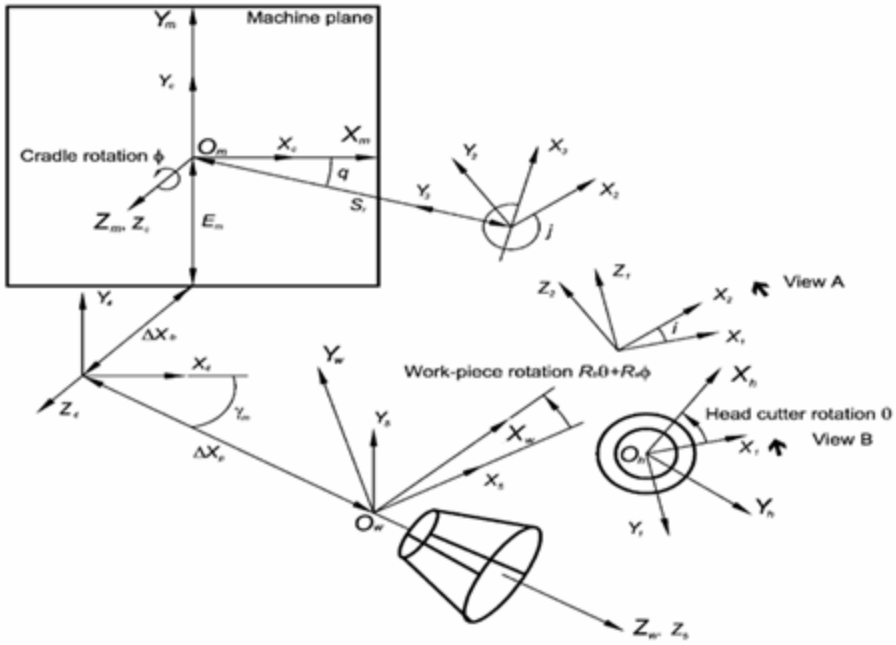

Fig. (7), Cutting machine setup for manufacturing a generated gear .

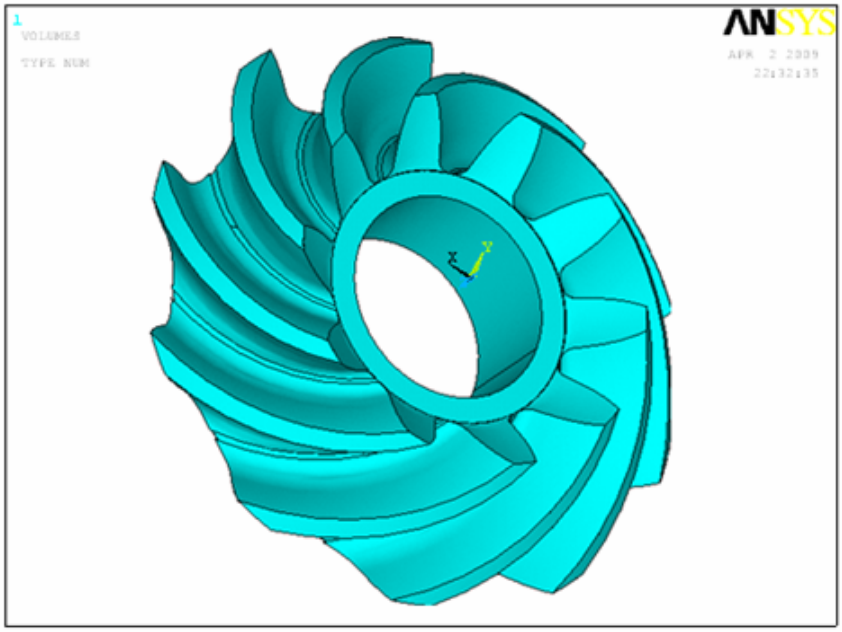

$\alpha = 22$ degree

$\beta = 37$ degree

$\gamma = 50$ degree

r =50 mm

$h_f = 4$ mm

$N_1 = 10$

Fig. (8), Hypoid pinion blank

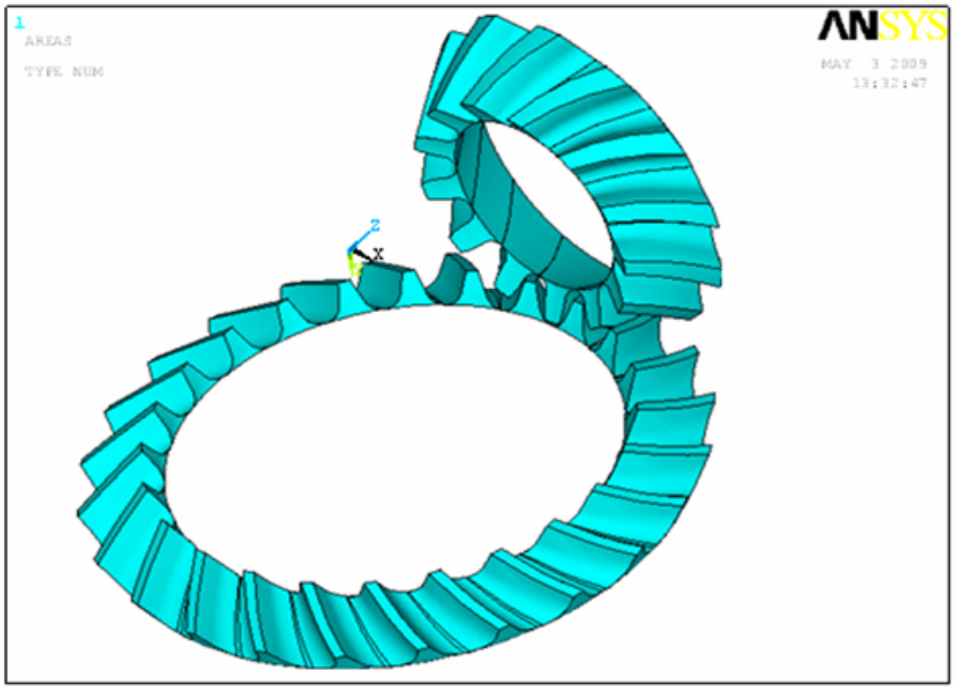

Fig. (9), Hypoid gear drive

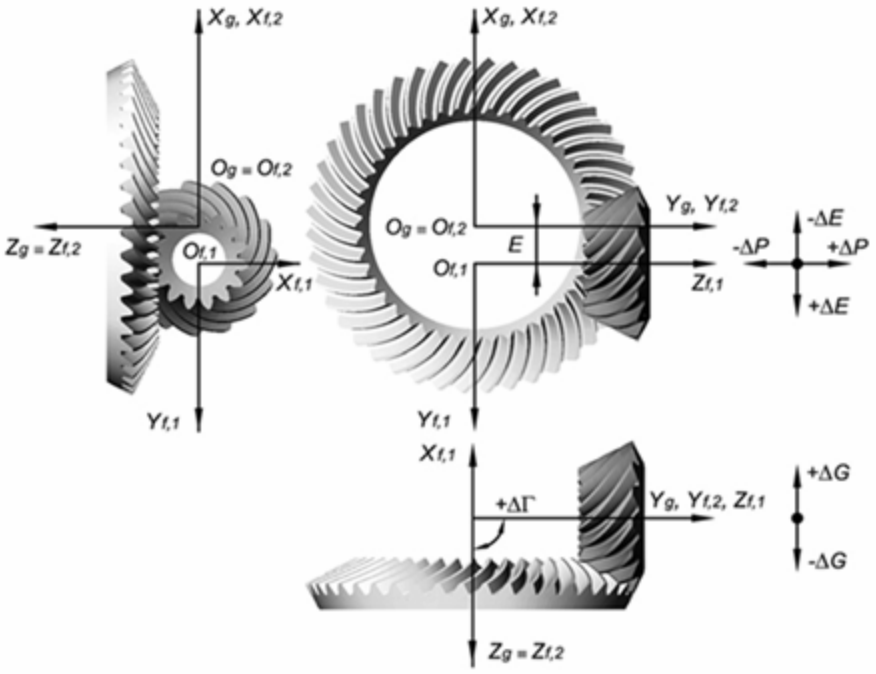

Fig. (10), Hypoid gear misalignment.

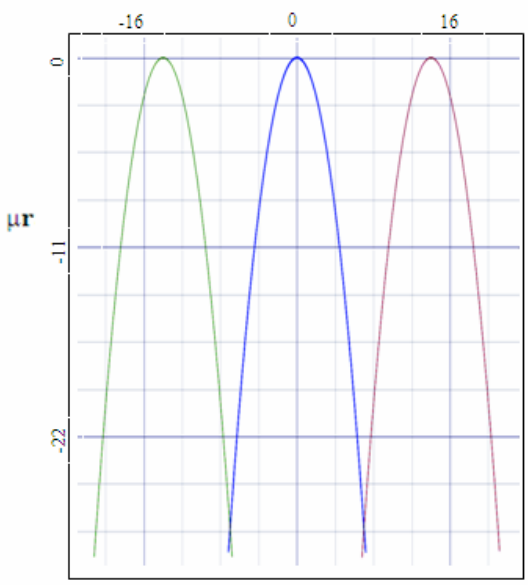

Fig. (11), Concave side transmission function, N_1=25

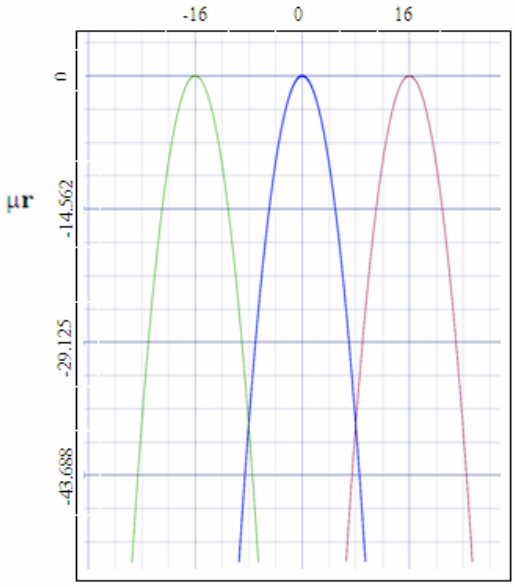

Fig. (12), Concave side transmission function, N_1=22

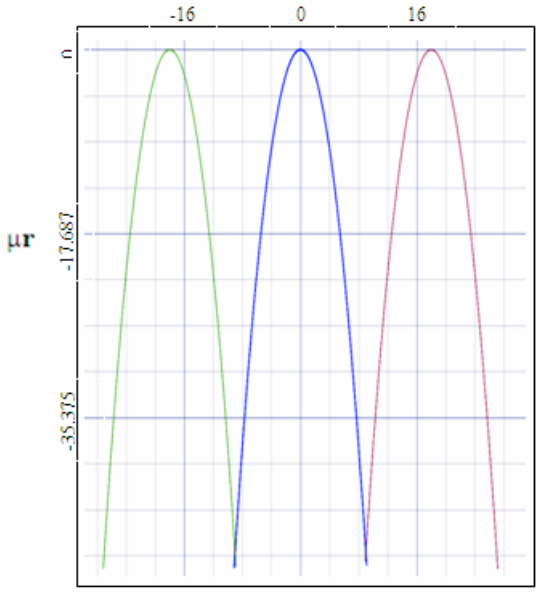

Fig. (13), Concave side transmission function, N_1=20

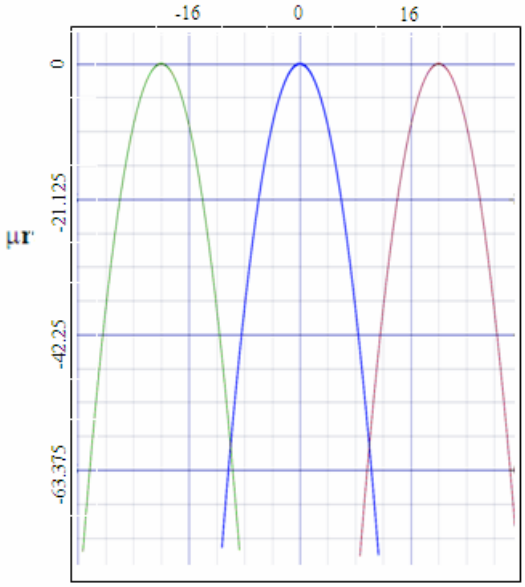

Fig. (14), Concave side transmission function, N_1=18

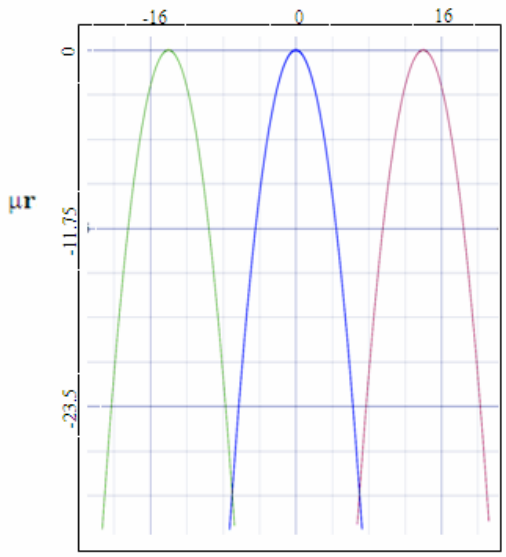

Pinion rotation angle (deg.)

Fig. (15), Convex side transmission function, N_1=25

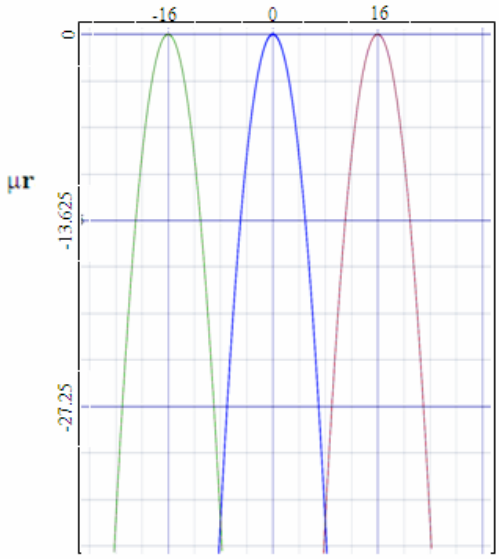

Pinion rotation angle (deg.)

Fig. (16), Convex side transmission function, N_1=22

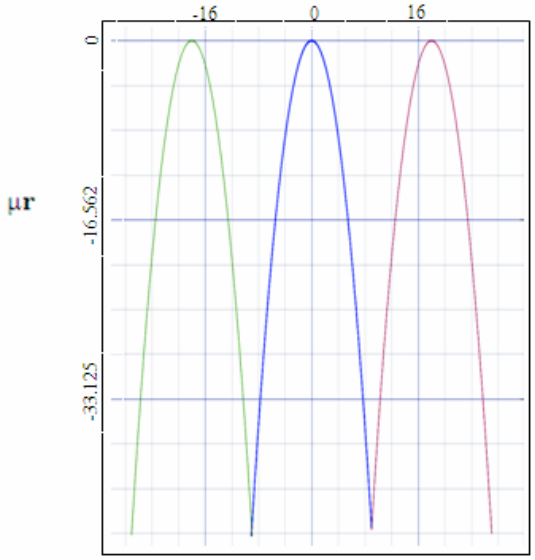

Pinion rotation angle (deg.)

Fig. (17), Convex side transmission function, N_1=20

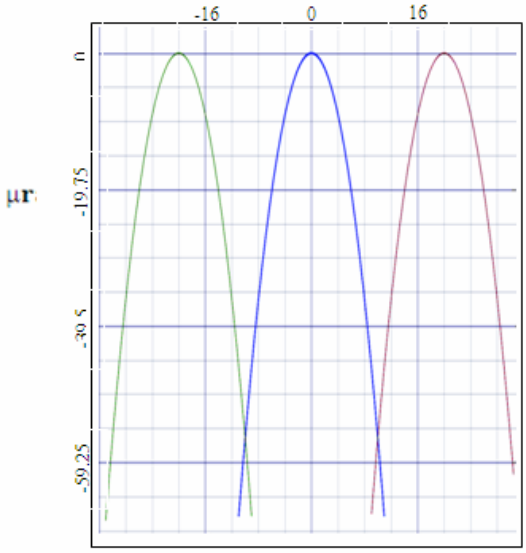

Pinion rotation angle (deg.)

Fig. (18), Convex side transmission function, N_1=18

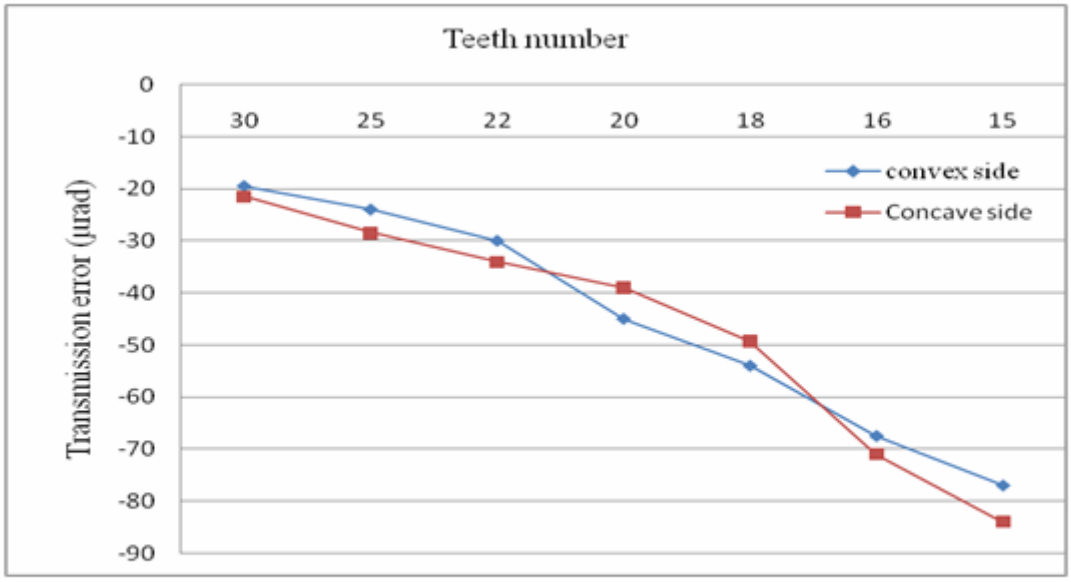

Fig. (19), Variation of transmission error with teeth number.